# Supplementary Materials for

# Title: An unprecedented mechanism of nucleotide methylation in organisms containing *thyX*

**Authors:** Tatiana V. Mishanina,[1,*] Liping Yu,[2] Kalani Karunaratne,[1] Dibyendu Mondal,[1] John M. Corcoran,[1] Michael A. Choi,[1] and Amnon Kohen[1,†]

**Affiliations:**

[1] Department of Chemistry, University of Iowa, Iowa City, IA 52242, USA.
[2] NMR Core Facility and Department of Biochemistry, Carver College of Medicine, University of Iowa, Iowa City, IA 52242, USA.

[†] Correspondence to: amnon-kohen@uiowa.edu

[*] This author's present address: Department of Biochemistry, University of Wisconsin-Madison, Madison, WI 53706, USA.

**TOC:**

**Materials and Methods:**

Chemicals were reagent grade and used as purchased without further purification, unless stated otherwise. 2′-deoxyuridine 5′-monophosphate (dUMP), glucose oxidase powder, D-glucose, $D_2O$, formaldehyde solution (36.5% by weight), and reduced nicotinamide adenine dinucleotide phosphate (NADPH) were obtained from Sigma-Aldrich. L-arginine was purchased from Sigma Life Sciences. Disodium Ethylenediamine Tetraacetate (EDTA) was obtained from Fisher Scientific. Non-radiolabeled *(6R)*-$N^5$,$N^{10}$-methylene-5,6,7,8-tetrahydrofolate and 5,6,7,8-tetrahydrofolate were provided by Eprova Inc. (Schaffhausen, Switzerland). Radiolabeled [2-$^{14}$C]-dUMP, $^{14}$C-formaldehyde, and [3′,5,7,9-$^3$H]-folic acid were purchased from Moravek Biochemicals. Radiolabeled folates were synthesized following published chemo-enzymatic protocol (*13*). Sodium dithionite powder was purchased from J.T. Baker. Tris(hydroxymethyl)aminomethane (Tris) and urea (carbamide) were obtained from Research Products International Corp. Radio- and stable-isotope-labeled FAD cofactors were enzymatically synthesized from riboflavin and ATP, as previously described (*11*). The FDTS from *Thermatoga maritima* (TM0449, GenBank accession number NP228259) was expressed and purified following the published procedure (*11*). The FDTS was reconstituted with isotopically labeled flavins as detailed elsewhere (*11*). *E. coli* dihydrofolate reductase for the synthesis of labeled folates was expressed and purified in house as described previously (*14*).

***Purification methods***

Prior to structural analyses, base-trapped intermediate was isolated from the crude quenched reactions via reverse-phase HPLC, in 50 mM potassium phosphate buffer, pH 6.0, containing 20% methanol. The elution of the trapped species was followed by the absorbance at 258 and 340 nm (the trapped derivative absorbs at both wavelengths, Fig. S4). The solution of the purified trapped compound was purged with argon to remove the methanol, freeze-dried and desalted via trituration into methanol.

***NMR spectroscopy***

The purified base-trapped intermediate was dissolved in 10 mM potassium phosphate, pD 6.1 (pH 6.5) in $D_2O$ for NMR studies. $^1$H homonuclear two-dimensional (2D) DQF-COSY (*15*), TOCSY (*16*), and ROESY (*17*) experiments, and $^1$H/$^{13}$C heteronuclear 2D HMQC, HMBC, and H2BC experiments (*18, 19*) were collected using a Bruker Avance II 800 MHz NMR spectrometer equipped with a sensitive cryoprobe. One dimensional (1D) $^{31}$P spectra and $^1$H/$^{31}$P heteronuclear 2D COSY spectra (*20*) were acquired on a Bruker Avance II 500 MHz NMR spectrometer. The NMR spectra were recorded at either 15 or 25$^o$C as indicated in the relevant text. The $^1$H chemical shifts were referenced to 2,2-dimethyl-2-silapentane-5-sulfonate (DSS), and the $^{13}$C and $^{31}$P chemical shifts were referenced using the frequency ratios as recommended by IUPAC (*21*). NMR spectra were processed using NMRPipe (*22*) and analyzed using NMRView (*23*).

***Data fitting for FDTS-catalyzed reaction kinetics***

The base-quench data were globally fitted to a kinetic model with one intermediate using Mathematica (Fig. 2, top panel):

$$\text{dUMP} \xrightarrow{k_1} I_1 \xrightarrow{k_2} \text{dTMP}$$

The following set of rate equations was used in the fitting:

$$\frac{d}{dt}[\text{dUMP}] = -k_1 \bullet [\text{dUMP}]$$

$$\frac{d}{dt}[I_1] = k_1 \bullet [\text{dUMP}] - k_2 \bullet [I_1]$$

$$\frac{d}{dt}[\text{dTMP}] = k_2 \bullet [I_1]$$

The acid-quench data from ref (*5*) were globally fitted to a two-intermediate model (Fig. 2, bottom panel):

$$\text{dUMP} \xrightarrow{k_1} I_1 \xrightarrow{k_2} I_2 \xrightarrow{k_3} \text{dTMP}$$

where the intermediate $I_1$ was assumed to be the one trapped by the base and hence the $k_1$ and $k_2$ rate constants (obtained from the one-intermediate fitting above) were held constant. The set of rate equations below was used in the fitting:

$$\frac{d}{dt}[\text{dUMP}] = -k_1 \bullet [\text{dUMP}]$$

$$\frac{d}{dt}[I_1] = k_1 \bullet [\text{dUMP}] - k_2 \bullet [I_1]$$

$$\frac{d}{dt}[I_2] = k_2 \bullet [I_1] - k_3 \bullet [I_2]$$

$$\frac{d}{dt}[\text{dTMP}] = k_3 \bullet [I_2]$$

***Preparation and activity tests of 5-deaza-5-carba-FAD-FDTS***

Holo-FDTS was first treated with a saturated solution of NaCl as previously described (*4, 11*), to remove most of the bound FAD. This enzyme was then denatured with 8 M urea solution at 4 ºC and dialyzed three times against 50 mM Tris-HCl buffer pH 8.0 containing 1 mM EDTA and 8 M urea, to remove any remaining FAD. The unfolded enzyme was further dialyzed three times against 50 mM Tris-HCl buffer pH 8.0, 1 mM EDTA and 500 mM L-arginine, to slowly refold the enzyme. Finally, the refolded arginine-free apo-FDTS was obtained by dialyzing the enzyme three times against 50 mM Tris-HCl buffer pH 8.0, 1 mM EDTA. All dialysis steps were carried out at 4 ºC**.** Apo-FDTS was then divided into two portions, and one half was reconstituted with FAD while the other with 5-deaza-FAD. Reconstituted enzymes were washed with 50 mM Tris-HCl buffer pH 8.0, 1 mM EDTA to remove any unbound cofactor. The concentration of the enzymes was measured spectrophotometrically (FAD $\varepsilon_{454}$ = 11,300 $M^{-1}$ $cm^{-1}$**,** 5-deaza-FAD $\varepsilon_{399}$ = 11,500 $M^{-1}$ $cm^{-1}$).

Activity assays were carried out on apo-FDTS (10 μM), FAD-reconstituted enzyme (1 μM), 5-deaza-FAD-FDTS **(**10 μM) and holo-enzyme (1 μM) at 65 ºC with 50:50 a mixture of cold:$^{14}$C-labeled dUMP (final specific radioactivity 26.6 mCi/ mmol), 50 μM $CH_2H_4$fol, 10 mM formaldehyde and 5 mM dithionite. Reactions were quenched after 15 min with liquid nitrogen, reactants and products were separated by analytical HPLC, and the radioactivity in the eluent was quantified by radioactivity flow detector Berthold FlowStar 513.

**Supplementary Discussion:**

*ThyX is a promising new target for antibiotic drugs with low toxicity*

Table S1 below presents examples of human pathogens containing *thyX*. Many pathogens strictly depend on *thyX* for thymine and thus DNA synthesis. All *Rickettsia* fall under this category, which include pathogens causing typhus, spotted fever, and other diseases that are now considered to be bioterrorism threats. Pathogens that contain *thyX* in addition to *Tdk* (coding for thymidine kinase) or *thyA* (coding for classical thymidylate synthase, TSase) can either scavenge thymidine from the host or synthesize it through an alternative pathway, respectively. These pathogens often develop multi-drug resistance, further emphasizing the importance of inhibiting *thyX* (FDTS). In the case of *M. tuberculosis*, for example, the bacterium contains both *thyA* and *thyX*, and under optimal growth conditions the expression of *thyA* exceeds that of *thyX* (*24*). However, *thyX* is essential for the pathogen's survival even under normal growth conditions, and compensates for the absence of thymine when TSase is blocked by an antibiotic drug, or when *thyA* is deleted from the bacterium genome altogether (*24*). As multi- and extreme-drug resistant tuberculosis becomes more common, the addition of an FDTS-inhibitor to the cocktail could prove essential for modern treatment.

Because the mechanisms contemplated until this point have been misleading, any rational drug design based on either crystal structures or chemical mechanisms have been quite hopeless. For example, our 2012 FDTS crystal structures with folates (PDB IDs 4GT9, 4GTA, and 4GTB) were misinterpreted to be dead-end complexes, and thus not looked at by the broad community for structure-based design. Some of the potential inhibitors that have electron-withdrawing substituents at C5 position on the uracil and 6-aza-uracil molecules have been synthesized and have shown weak inhibition (*25-27*), since no nucleophilic activation of uracil is in fact necessary. The new mechanism proposed here not only provides a roadmap for rational drug design, but also emphasizes the dramatic differences between the *thyA*-encoded human enzyme and FDTS, lending hope that inhibitors of the latter will not affect the human enzyme and will have little or no toxicity.

One possible route to FDTS inhibition could take advantage of flavin's nucleophilicity toward folate proposed in the current mechanism. For instance, a series of folate-based compounds with strongly electrophilic substituents at N5 (e.g., epoxide, alkyl halide, formyl, etc.), or such substituents on a 5-deaza folate, could inactivate FDTS via formation of stable flavin-folate adducts.

*The mechanism of intermediates' degradation*

Fig. S10 outlines the possible routes from the proposed flavin-bound reaction intermediate (Fig. 4) to the isolated quencher-modified species. The bridged intermediate $I_1$ would become deprotonated at C5 of uracil upon basic quench, to yield the trapped derivative (Fig. 3); in acid, protonation of the flavin's N5 and water attack at C7 methylene will substitute FAD with a hydroxyl to produce 5-hydroxymethyl-dUMP (Fig. S10). Water addition to the exocyclic methylene of $I_2$ would also lead to 5-hydroxymethyl-dUMP in acidic quench, as described elsewhere (*5*). The basic quench, on the other hand, induces a fast "collapse" of $FADH^-$ onto C7 of $I_2$, leading to its reduction to dTMP faster than the denaturation of the protein, and long before it would have been reduced under normal reaction conditions. This base-induced conversion takes place within the mixing time of the quench-flow instrument (< 2 ms), occurs after the decay of $I_1$, and coincides with the formation and disappearance of $I_2$. At 25 ˚C, a temperature that is much lower than the *T. maritima* physiological optimum (85 ˚C), and a normal turnover pH, the much slower dTMP formation is in accordance with the low-temperature reversible reduction of $I_2$ at C6 to form $I_3$ (Fig. S9). Since at a temperature closer to physiological for *Tm*FDTS (e.g., 65 ˚C), no deuterium is found at C6 of the product dTMP (*7*), it is likely that $I_2$ does not accumulate under physiological conditions and is reduced solely at C7 to form the product.

The described ability of the reduced flavin to function as a methylene carrier calls for a unique protein architecture of FDTS, distinct from flavoenzymes that exclusively specialize in redox chemistry. Indeed, when the structure of FDTS was first determined, a structural similarity search with FDTS coordinates failed to detect significant similarities to any other protein structure, indicating that FDTS exhibits a novel fold (*28*). A year later, a novel helix-loop-strand FAD binding motif was identified in FDTS proteins (*4*), distinct from FAD-binding folds found in other redox flavoenzymes, e.g., glutathione reductase, ferredoxin reductase, and pyruvate oxidase families.

*Structure of base-trapped intermediate by NMR*

This section elaborates on the structural features of the base-trapped intermediate derivative untouched in the main text of the report. The structure is presented in the top panel of Fig. 3, and the atomic numbering follows that of the relevant reactants. The nucleotide-originated moiety is labeled as subunit U (red) and includes the transferred $CH_2H_4$fol-originated methylene (black), while the flavin-originated moiety is marked as subunit F (blue). The F1′ $CH_2$ group of ribitol sugar on the F-subunit exhibits detectable HMBC connectivity to FC9a and FC10a (Fig. 3, bottom panel), although these cross peaks are relatively weak, possibly due to the flexible rotation of the FN10-FC1′ bond. In fact, all HMBC cross peaks for F1′, F2′, and F3′ are very weak, likely due to the flexibility in this part of the structure. These data show that the chemically-modified isoalloxazine core of the flavin has been degraded to 6,7-dimethyl-2,3-dioxoquinoxaline under the base-quench conditions. The determined chemical shifts of F6, F7, F7a$CH_3$, F5a, and F4a are very similar to those of F9, F8, F8a$CH_3$, F9a, and F10a, respectively, consistent with the ring pseudo-symmetry of the determined decomposed flavin structure. Furthermore, the bridging methylene protons (UH7) display strong NOEs to both the aromatic H6 proton (FH6) on the decomposed flavin and uracil's H6 proton (UH6) in the ROESY spectrum (Fig. S6).

*Is it possible that the flavin is not chemically modified during normal activity and is bound to the nucleotide solely due to the basic quench?* No: incubations of oxidized or reduced FAD-FDTS under the base-quenching conditions did not cause any damage to the flavin's isoalloxazine ring. The ring only falls apart when chemically treated during the course of the reaction, indicating that the flavin must have been covalently modified *prior* to the introduction of the base. Isoalloxazine degradation is not unprecedented; there exist literature examples of either enzyme-catalyzed (*29-31*) or chemically induced (*32-34*) isoalloxazine core cleavage. In the studies of methanol oxidase, an FAD-dependent enzyme, an initial covalent adduct between cyclopropanol suicide substrate and the flavin was converted to 1-(ribityldiphosphoadenosine)-4-(3-hydroxypropyl)-2,3-dioxoquinoxaline upon $NaBH_4$ treatment under basic conditions (*30*). The dioxoquinoxaline is also a known product of bacterial riboflavin degradation (*29*).

There are two well-separated $^{31}$P peaks resonated at 3.29 and 18.00 ppm in the 1D $^{31}$P NMR spectrum of the base-trapped intermediate (Fig. S7A). The $^{31}$P peak at 3.29 ppm displays COSY cross peaks to the deoxyribose H5′ protons of dUMP, while the $^{31}$P peak at 18.00 ppm has COSY cross peaks to the ribitol H4′ proton and H5′ protons of the degraded FAD (Fig. S7B). Therefore, these two $^{31}$P peaks correspond to dUMP monophosphate and ribitol 4′,5′-cyclic phosphate, respectively. The $^{1}$H and $^{13}$C chemical shifts of F4′ and F5′ groups are strongly downfield shifted, which is consistent with the formation of 4′,5′-cyclic phosphate. The observed $^{31}$P chemical shift of the ribitol 4′,5′-cyclic phosphate at 18.00 ppm is also consistent with the literature reports of similar cyclic phosphates (*35, 36*). Therefore, under the base-quench conditions employed in this study, FAD has lost its AMP tail to form 4',5'-cyclic phosphate. The hydrolysis of the pyrophosphate bond and phosphate cyclization is not surprising as under alkaline condition FAD is known to form AMP and 4',5'-cyclicphospho FMN (*37, 38*).

*Detection limits in the activity assays of apo- and 5-deaza-FAD-reconstituted FDTS*

The removal of FAD from FDTS by salting-out as described in the past (*4*), resulted in residual activity (1-10% of the original holo-FDTS activity). In our hands, this residual activity is identical to that of the same "apo-enzyme" reconstituted with 5-deaza-FAD, which made it difficult to determine definitively whether it is inactive. However, when this salted-out enzyme was further denatured by 8 M urea, followed by removal of FAD and protein refolding, neither the apo-enzyme nor the enzyme reconstituted with 5-deaza-FAD presented any detectable activity (Figs. S9B and S9C, respectively), while apo-FDTS after reconstitution with FAD regained the activity equivalent to holo-FDTS (Fig. S9A). The detection limit of 1/250,000 (S/N) was determined by comparing the background (7 dpm) to the total radioactivity per HPLC injection (173326.40 dpm), and adding a factor of 10 for the 10-fold higher enzyme concentration used when analyzing the apo-enzyme and enzyme reconstituted with 5-deaza-FAD.

**Supplementary Figures**

**Fig. S1.** Intermediate trapping with radiolabeled nucleotide and folate substrates. Shown are the HPLC radiograms of FDTS reactions quenched with 1 M NaOH after 1 s reaction with [2-$^{14}$C]-dUMP (A) and [11-$^{14}$C]-$CH_2H_4$fol (B). The same chemical species is trapped in both cases (35 min elution time), indicating that this species contains both the pyrimidine moiety of dUMP and the methylene of $CH_2H_4$fol cofactor.

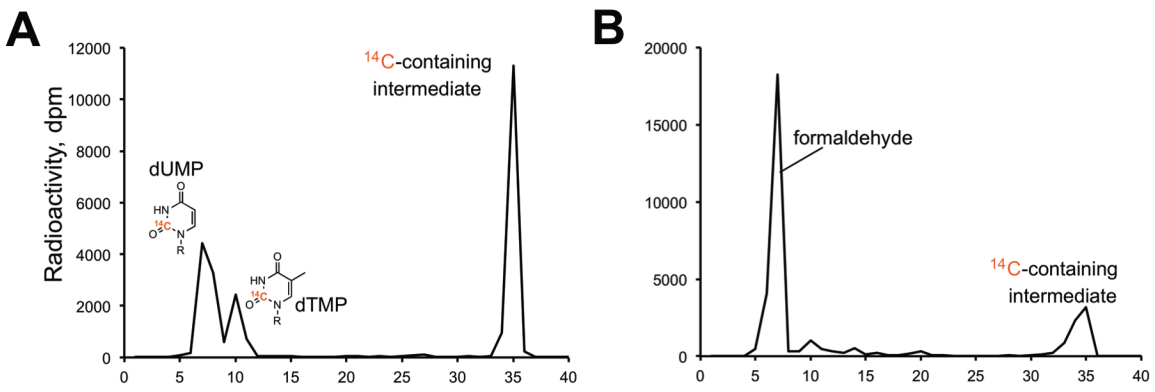

**Fig. S2.** High resolution ESI-MS (A, C) and MS/MS (B) of the base-trapped intermediate isolated in the reactions with (A, B) unlabeled FAD-FDTS and (C) [Dioxopyrimidine-$^{13}$C,$^{15}$N]-FAD-FDTS. Dioxopyrimidine is the ring C of isoalloxazine (see Fig. S5A). A 2 dalton mass shift is observed with isotopically labeled flavin, consistent with incorporation of the two $^{13}$C carbons of the isoalloxazine (C4a and C10a) into the intermediate. The spectra were collected in the negative-ion mode.

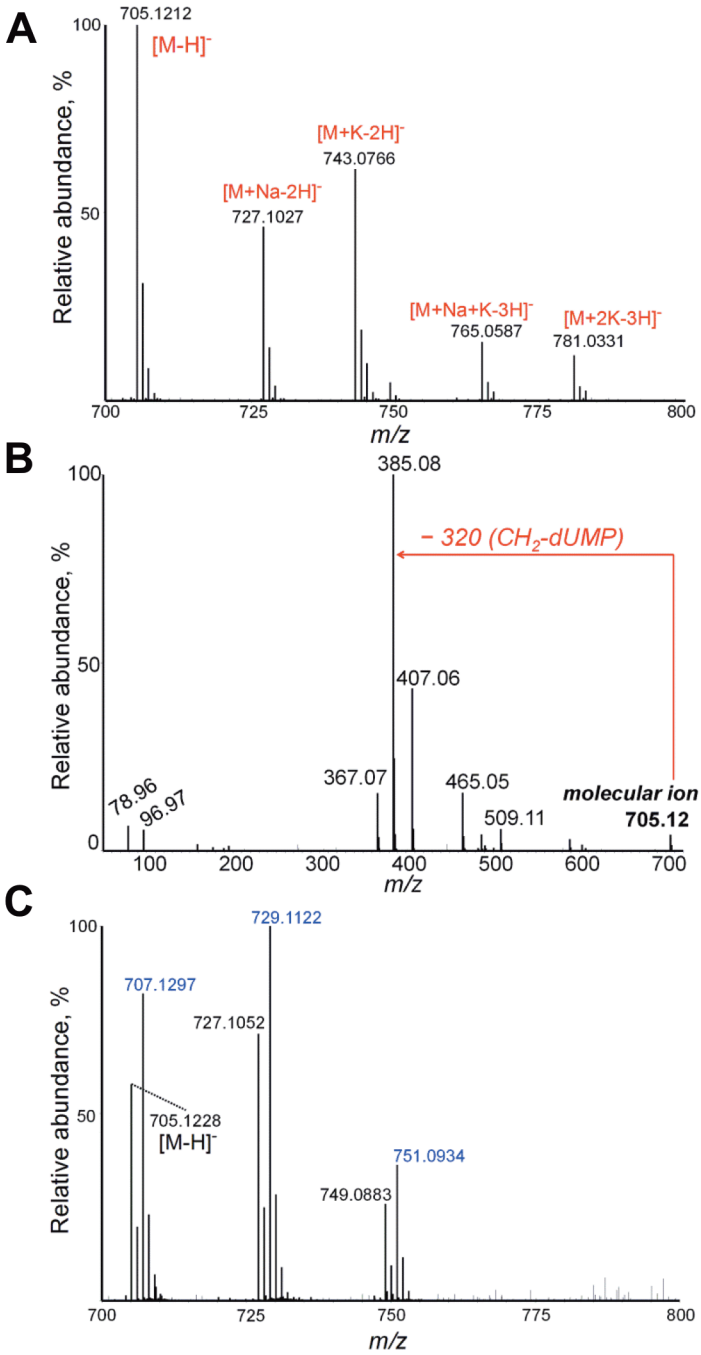

**Fig. S3.** Chemical mechanisms for FDTS proposed to date. Methylene is postulated to be delivered to dUMP by methylenetetrahydrofolate ($CH_2H_4$folate) directly. (A) dUMP reduction by the flavin precedes the methylene transfer from $CH_2H_4$folate (*7*); (B) hydride transfer occurs after the methylene placement (*5, 9*).

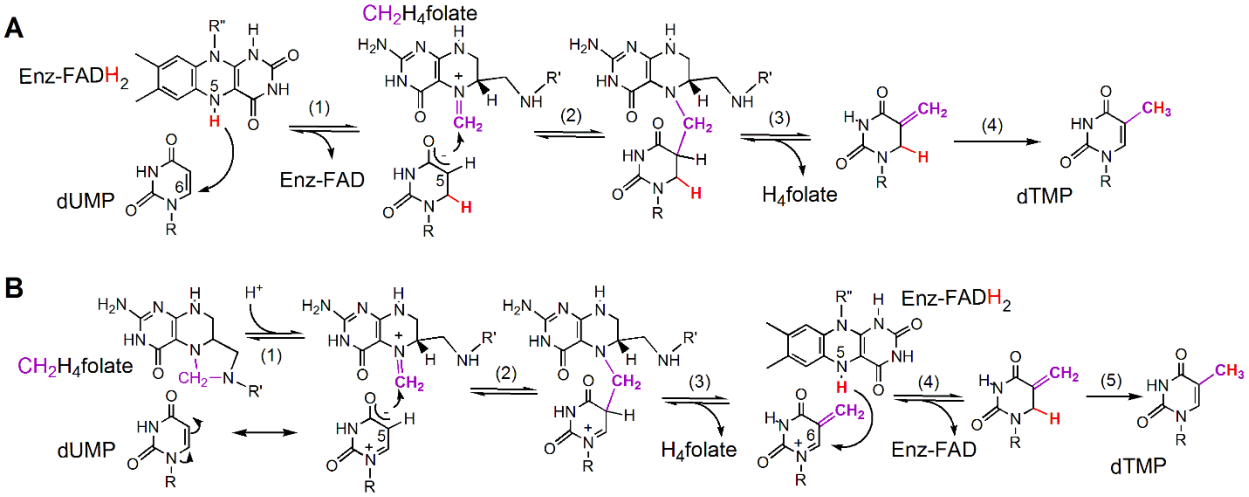

**Fig. S4.** UV-vis absorbance spectrum of the purified base-trapped intermediate.

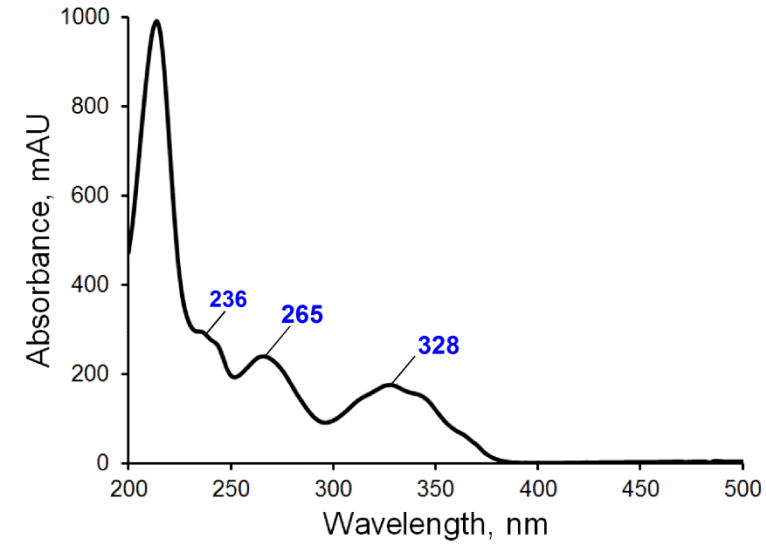

**Fig. S5.** FAD nomenclature and flavin-bound base-trapped intermediate. (A) Flavin adenine dinucleotide (FAD) chemical structure and its atomic numbering and nomenclature used in the main text. Ring C of the isoalloxazine is referred to as "dioxopyrimidine." (B) HPLC radiogram of [7a,8a-$^{3}$H]-FAD-FDTS reaction with [2-$^{14}$C]-dUMP quenched at 1 s with 1 M NaOH. An elution profile different than the one in Fig. S1 was used, so the trapped-intermediate elutes earlier in the chromatogram (15 min). The trapped intermediate derivative clearly contains the labeled dimethylbenzene portion of FAD.

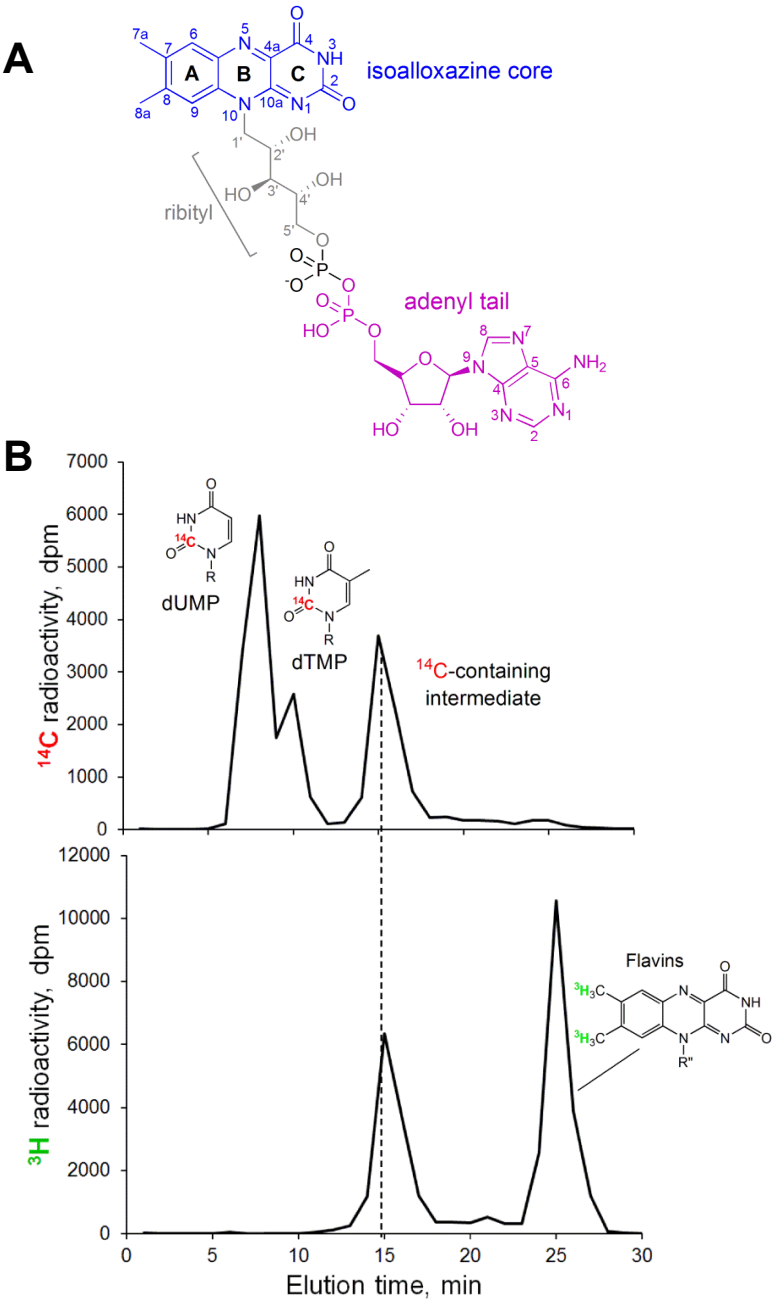

**Fig. S6.** NMR analysis of the base-trapped intermediate. (*Top*) $^{1}H/^{13}C$ HMQC spectrum acquired at 15°C with a $^{13}C$ sweep width of 20,000 Hz (corresponding to a range of 99.388 ppm) and $^{13}C$ carrier set at 85.0 ppm. The folded cross peaks are shown in red. The cross peaks labeled with a single star and double stars are derived from residual Tris buffer and sample impurity, respectively. (*Bottom*) 2D ROESY spectrum acquired at 15˚C with a mixing time of 300 ms. Clearly, the $CH_2H_4$fol-drived methylene protons (UH7) display strong NOEs to the F-subunit aromatic proton FH6 and the U-subunit aromatic proton UH6 (circled in red), consistent with the determined structure.

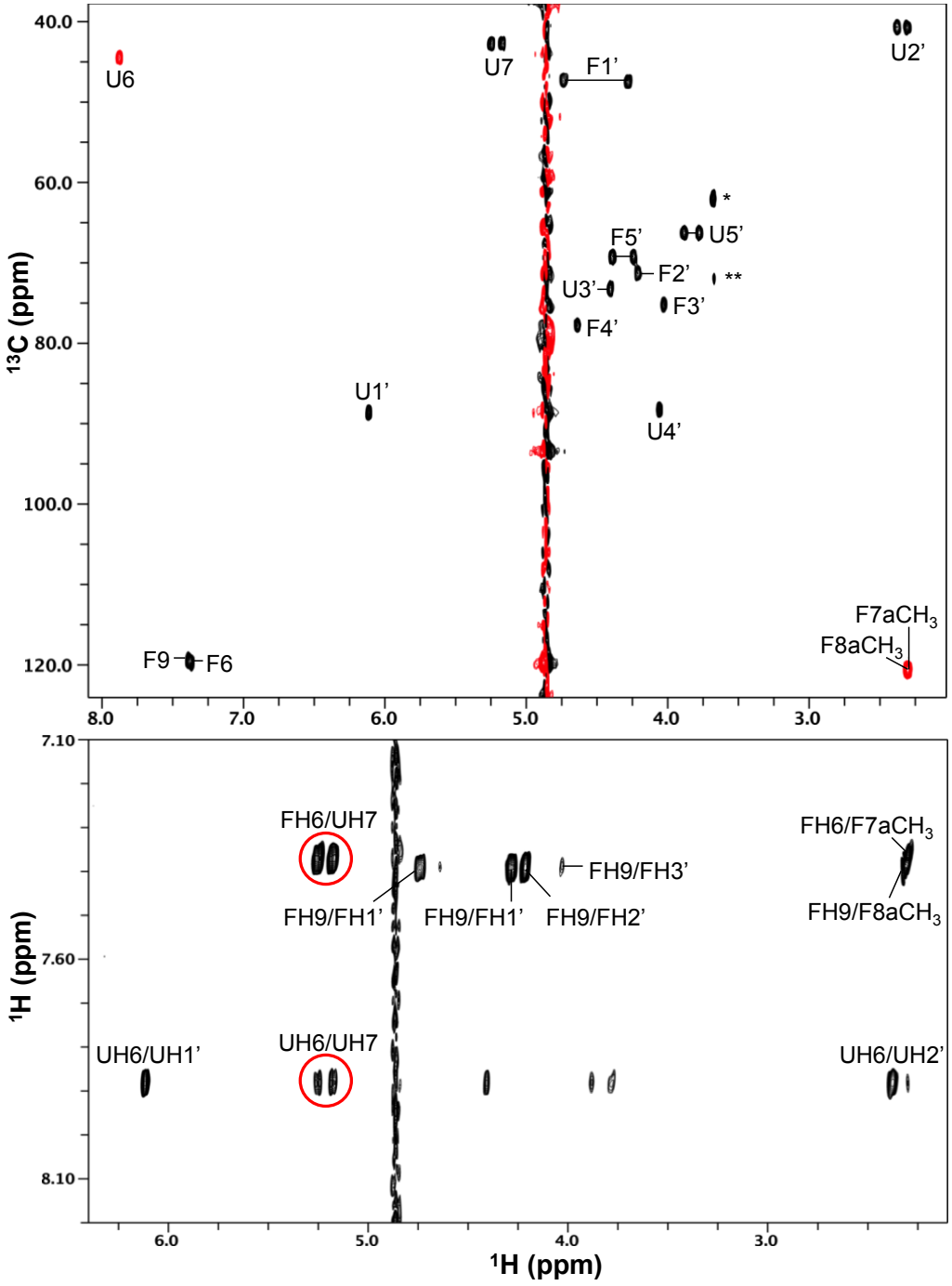

**Fig. S7.** 1D $^{31}$P NMR spectrum (A) and 2D $^{1}$H/$^{31}$P COSY spectrum (B) of the base-trapped intermediate acquired at 25$^{o}$C. The positive and negative peaks of the 2D $^{1}$H/$^{31}$P COSY spectrum are in black and red, respectively.

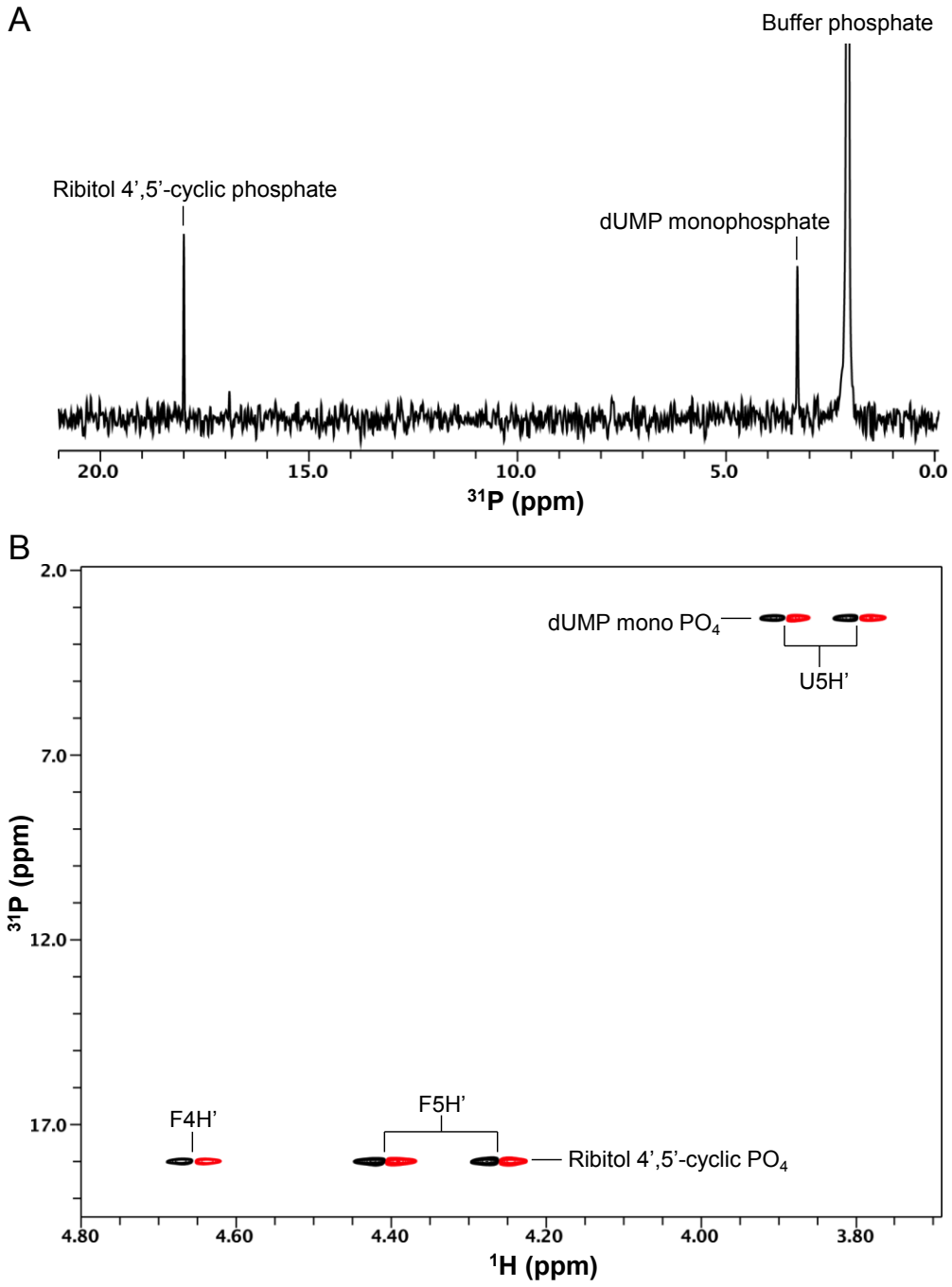

**Fig. S8.** Detailed chemical mechanism proposed for FDTS based on current findings. The numbering of steps in the flavin oxidative half-reaction follows that in the main text. Green arrows represent a side reaction of *Tm*FDTS that accounts for $D_2O$ deuterium found at C6 of dTMP product at sub-physiological temperatures. In all low-temperature crystal structures of *Tm*FDTS, N5 of FAD is located between C5 and C6 of dUMP (~3.4 Å), and would be too far from the exocyclic methylene (C7) of $I_2$ for efficient hydride transfer to this position (red arrows). In such situations, reduction of $I_2$ at C6 (green arrows) would lead to formation of an isomer of dTMP ($I_3$), whose direct isomerization to dTMP would be expected to be extremely slow (since thermal 1,3-sigmatropic rearrangement is quantum-mechanically forbidden), and reversible re-oxidation by the FAD is most likely. Eventually, $I_2$ would be reduced irreversibly at C7 to form the dTMP product (red arrow). At close to physiological temperature, however, no such side reaction seems to happen, as no deuterium was found at C6 of dTMP (all in C7, as expected) (*7*).

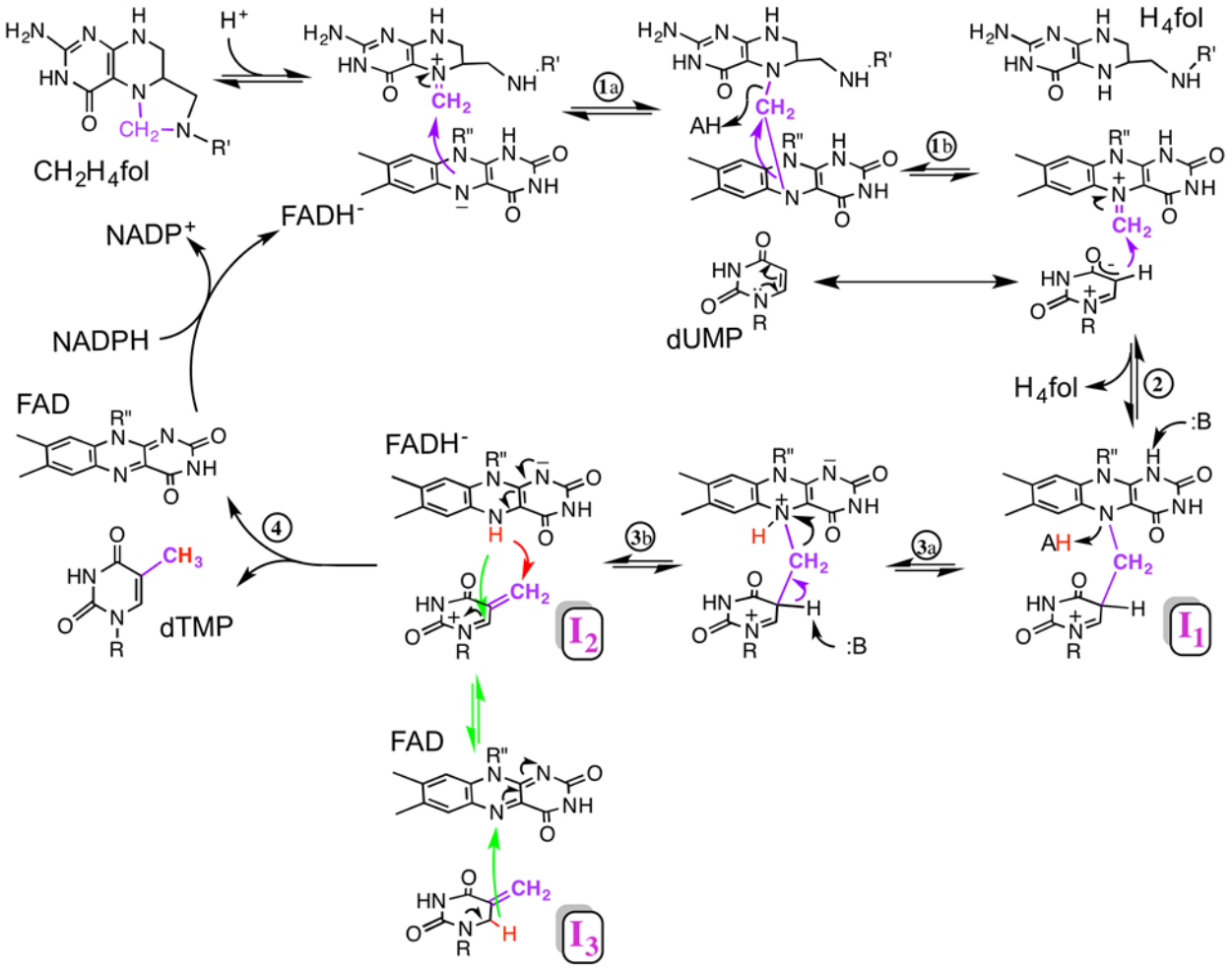

**Fig. S9.** Activity tests of 5-deaza-5-carba-FAD-FDTS. Apo-FDTS was prepared by urea denaturation method, as described in the text. All reactions were carried out at 65 ºC for 15 min with a 50:50 mixture of cold:[2-$^{14}$C]-dUMP, 50 µM $CH_2H_4$fol, 10 mM formaldehyde and 5 mM dithionite. Shown are reactions of: (A) FAD-reconstituted FDTS (1 µM); (B) 5-deaza-5-carba-FAD-FDTS (10 µM), and (C) apo-enzyme (10 µM). Apo-FDTS and 5-deaza-FAD-FDTS did not show any activity, while FAD-reconstituted FDTS showed 29% dUMP to dTMP conversion, which is comparable with that of the holo-enzyme under identical conditions (not shown). Based on the S/N of the radiograms and the 1:10 ratio of the FAD reconstituted enzyme to the apo- or 5-deaza-FAD-reconstituted enzyme, the detection limit is 1/250,000 as discussed in the Supplementary Discussion.

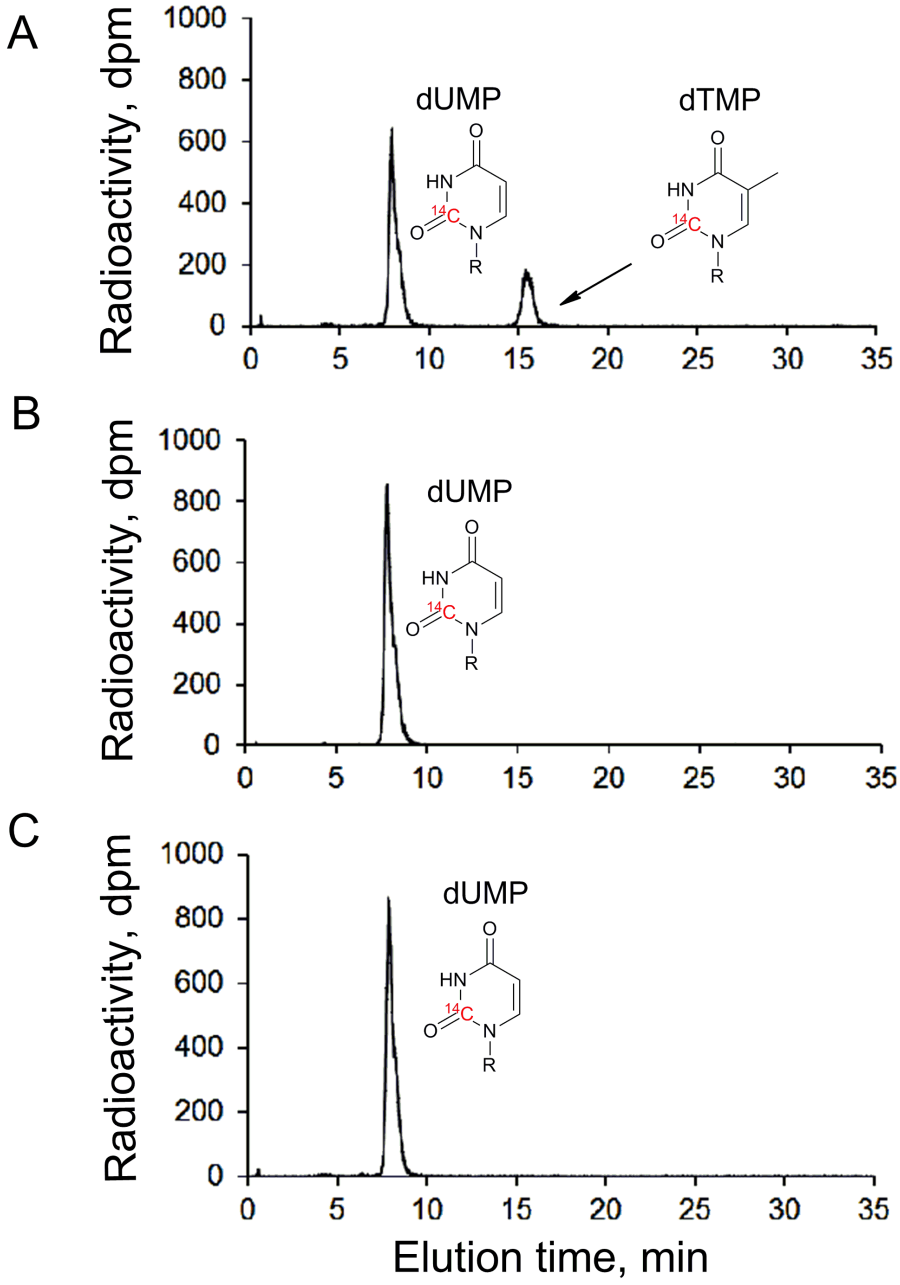

**Fig. S10.** Trapping mechanisms of the putative covalent flavin intermediate $I_1$ in aerobic acidic and basic quenchers. R, 2'-deoxyribose-5'-phosphate; R", adenosine-5'-pyrophosphate-ribityl.

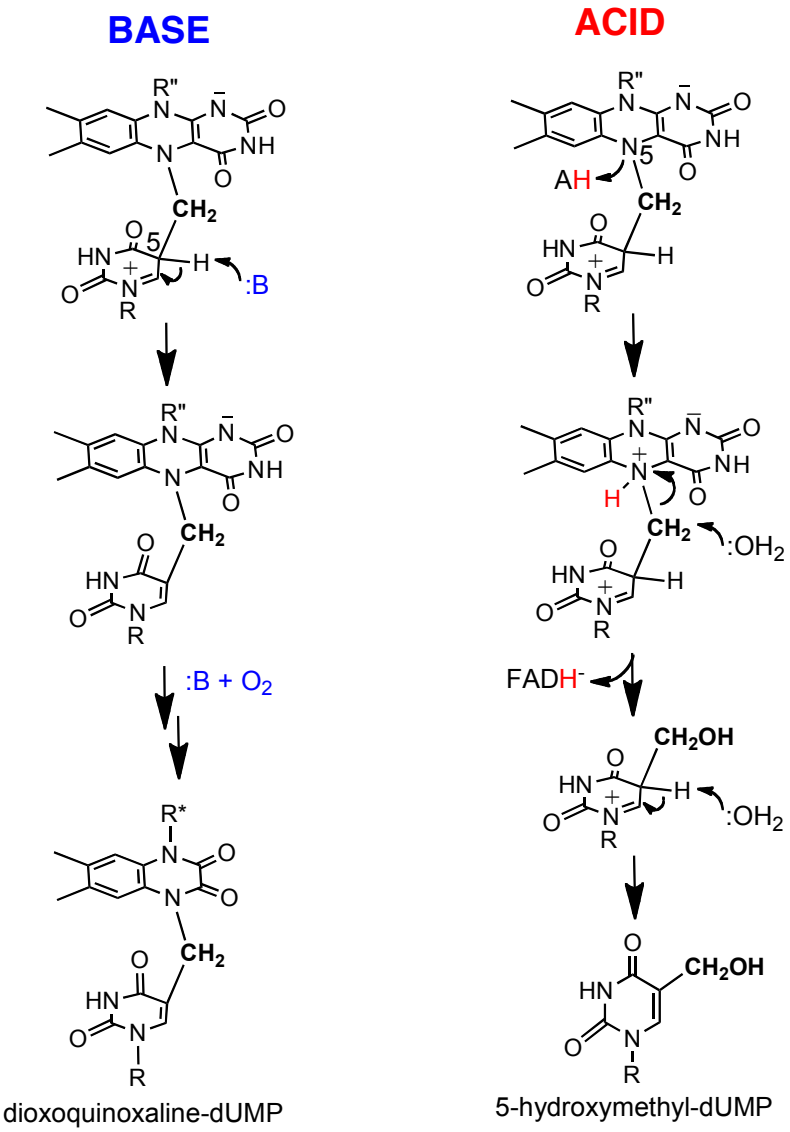

**Supplementary Tables**

**Table S1.** Examples of human pathogenic bacterial species containing *thyX*-encoded thymidylate synthase (FDTS). Adapted from ref (*2*). Occurrence of thymidine kinase (Tdk) and canonical thymidylate synthase (ThyA) is indicated, as reported in 2014-updated version of Clusters of Orthologous Groups (COG) database: http://www.ncbi.nlm.nih.gov/COG/. The roles of these genes and their relations to *thyX* are discussed in the Supplementary Discussion.

| Bacterial species | Associated disease(s) | Tdk | ThyA |
|---|---|---|---|
| *Bacillus anthracis* | anthrax | + | + |
| *Borrelia burgdorferi* | Lyme disease | + | - |
| *Campylobacter jejuni* | diarrhea | - | - |
| *Chlamydia trachomatis* | trachoma | - | - |
| *Chlamydia pneumoniae* | pneumonia | - | - |
| *Clostridium botulinum* | botulism | + | + |
| *Helicobacter pylori* | stomach ulcer, gastric cancer | - | - |
| *Mycobacterium leprae* | leprosy | - | + |
| *Mycobacterium tuberculosis* | tuberculosis | - | + |
| *Rickettsia prowazeki* | typhus | - | - |
| *Rickettsia rickettsii* | spotted fever | - | - |
| *Treponema pallidum* | syphilis | - | - |

**Table S2.** Chemical shifts (ppm) of the signals in the $^{1}H$, $^{13}C$, and $^{31}P$ NMR spectra of the base-trapped intermediate in FDTS reaction quenched with 0.3 N NaOH (final concentration) after 1s.

| | | $^{1}H/^{13}C/^{31}P$ (ppm)[a] | | | | | | |
|---|---|---|---|---|---|---|---|---|
| Residues | | 1 | 2 | 3 | 4 | 5 | 6 | 7 |
| **$CH_2$-dUMP subunit (U)** | | | | | | | | |
| Ribose | $^{1}H$ | 6.114 | 2.306 | 4.405 | 4.058 | 3.779 | | |
| | $^{1}H$ | - | 2.378 | - | - | 3.881 | | |
| | $^{13}C$ | 88.60 | 40.71 | 73.34 | 88.26 | 66.31 | | |
| Uracil | $^{1}H$ | - | - | - | - | - | - | 5.167 |
| | $^{1}H$ | - | - | - | - | - | 7.880 | 5.246 |
| | $^{13}C$ | - | 153.71 | - | 167.04 | 110.78 | 143.84 | 42.71 |
| Phosphate | $^{31}P$ | 3.29[b] | | | | | | |
| **Flavin-derived subunit (F)** | | | | | | | | |
| Ribitol | $^{1}H$ | 4.277 | 4.209 | 4.208 | 4.640 | 4.242 | | |
| | $^{1}H$ | 4.737 | - | - | - | 4.391 | | |
| | $^{13}C$ | 47.47 | 71.28 | 75.35 | 77.79 | 69.21 | | |

| Aromatic[c] | Position | 4a | 5a | 6 | 7 | 8 | 9 | 9a | 10a | F7a$CH_3$ | F8a$CH_3$ |
|---|---|---|---|---|---|---|---|---|---|---|---|
| | $^{1}H$ | - | - | 7.368 | - | - | 7.390 | - | - | 2.302 | 2.317 |
| | $^{13}C$ | 158.53 | 126.20 | 119.81 | 136.67 | 137.12 | 119.44 | 126.65 | 158.75 | 21.22 | 21.22 |
| Phosphate | $^{31}P$ | 18.00[d] | | | | | | | | | |

[a] Chemical shifts at 15°C in 10 mM potassium phosphate, pH 6.1.

[b] Chemical shift at 25°C for the dUMP monophosphate.

[c] The aromatic portion is 6,7-dimethyl-2,3-dioxoquinoxaline. Here, however, we used conventional flavin atomic numbering (see Fig. S5A), to simplify tracking of the flavin nucleotide decomposition.

[d] Chemical shift at 25°C for the ribitol 4',5'-cyclic phosphate.

**Supplementary References:**


1. H. Myllykallio *et al.*, An alternative flavin-dependent mechanism for thymidylate synthesis., *Science* **297**, 105-107 (2002).
2. D. Leduc *et al.*, Two distinct pathways for thymidylate (dTMP) synthesis in (hyper)thermophilic Bacteria and Archaea, *Biochem. Soc. Trans.* **32**, 231-235 (2004).
3. S. A. Lesley *et al.*, Structural genomics of the Thermotoga maritima proteome implemented in a high-throughput structure determination pipeline, *Proceedings of the National Academy of Sciences of the United States of America* **99**, 11664-11669 (2002).
4. I. I. Mathews *et al.*, Functional analysis of substrate and cofactor complex structures of a thymidylate-synthase complementing protein., *Structure (Camb.)* **11**, 677-690 (2003).
5. T. V. Mishanina *et al.*, Trapping of an intermediate in the reaction catalyzed by flavin-dependent thymidylate synthase (FDTS), *J. Am. Chem. Soc.* **134**, 4442-4448 (2012).
6. T. V. Mishanina, J. M. Corcoran, A. Kohen, Substrate Activation in Flavin-Dependent Thymidylate Synthase, *J. Am. Chem. Soc.* **136**, 10597-10600 (2014).
7. E. M. Koehn *et al.*, An unusual mechanism of thymidylate biosynthesis in organisms containing the *thyX* gene., *Nature* **458**, 919-924 (2009).
8. E. M. Koehn *et al.*, Folate binding site of flavin-dependent thymidylate synthase, *Proc. Natl. Acad. Sci. U. S. A.* **109**, 15722-15727 (2012).
9. J. A. Conrad, M. Ortiz-Maldonado, S. W. Hoppe, B. A. Palfey, Detection of Intermediates in the Oxidative Half-Reaction of the FAD-Dependent Thymidylate Synthase from Thermotoga maritima: Carbon Transfer without Covalent Pyrimidine Activation, *Biochemistry* **53**, 5199-5207 (2014).
10. C. W. Carreras, D. V. Santi, The catalytic mechanism and structure of thymidylate synthase., *Annu. Rev. Biochem.* **64**, 721-762 (1995).
11. T. V. Mishanina, A. Kohen, Synthesis and application of isotopically labeled flavin nucleotides, *J. Label. Compd Radiopharm.* **58**, 370-375 (2015).
12. D. Hamdane, M. Argentini, D. Cornu, B. Golinelli-Pimpaneau, M. Fontecave, FAD/folate-dependent tRNA methyltransferase: flavin as a new methyl-transfer agent, *J. Am. Chem. Soc.* **134**, 19739-19745 (2012).
13. N. Agrawal, C. Mihai, A. Kohen, Microscale synthesis of isotopically labeled *R*-[6-$^{x}$H]$N^{5}$,$N^{10}$-methylene-5,6,7,8-tetrahydrofolate as a cofactor for thymidylate synthase, *Anal. Biochem.* **328**, 44-50 (2004).
14. G. P. Miller, S. J. Benkovic, Deletion of a highly motional residue affects formation of the Michaelis complex for Escherichia Coli dihydrofolate reductase., *Biochemistry* **37**, 6327-6335 (1998).
15. M. Rance *et al.*, Improved spectral resolution in COSY 1H NMR spectra of proteins via double quantum filtering, *Biochemical and Biophysical Research Communications* **117**, 479-485 (1983).
16. L. Braunschweiler, R. R. Ernst, Coherence transfer by isotropic mixing: Application to proton correlation spectroscopy, *J. Magn. Reson.* **53**, 521-528 (1983).

17. J. Jeener, B. H. Meier, P. Bachmann, R. R. Ernst, Investigation of exchange processes by two-dimensional NMR spectroscopy, *J. Chem. Phys.* **71**, 4546-4553 (1979).

18. B. O. Petersen *et al.*, H2BC: a new technique for NMR analysis of complex carbohydrates, *Carbohydr. Res.* **341**, 550-556 (2006).

19. N. T. Nyberg, J. O. Duus, O. W. Sørensen, Editing of H2BC NMR spectra, *Magn. Reson. Chem.* **43**, 971-974 (2005).

20. K. V. R. Chary, V. K. Rastogi, G. Govil, An Efficient 2D NMR Technique HELCO for Heteronuclear [31P-1H] Long-Range Correlation, *J. Magn. Reson. Series B* **102**, 81-83 (1993).

21. R. K. Harris *et al.*, Further conventions for NMR shielding and chemical shifts (IUPAC Recommendations 2008), *Pure Appl. Chem.* **80**, 59-84 (2008).

22. F. Delaglio *et al.*, NMRPipe: A multidimensional spectral processing system based on UNIX pipes, *J. Biomol. NMR* **6**, 277-293 (1995).

23. B. A. Johnson, R. A. Blevins, NMR View: A computer program for the visualization and analysis of NMR data, *J. Biomol. NMR* **4**, 603-614 (1994).

24. A. S. Fivian-Hughes, J. Houghton, E. O. Davis, *Mycobacterium tuberculosis* thymidylate synthase gene *thyX* is essential and potentially bifunctional, while *thyA* deletion confers resistance to *p*-aminosalicylic acid, *Microbiol.* **158**, 308–318 (2012).

25. M. Kögler *et al.*, Synthesis and Evaluation of 5-Substituted 2′-deoxyuridine Monophosphate Analogues As Inhibitors of Flavin-Dependent Thymidylate Synthase in Mycobacterium tuberculosis, *Journal of Medicinal Chemistry* **54**, 4847-4862 (2011).

26. M. Kögler *et al.*, Synthesis and Evaluation of 6-Aza-2′-deoxyuridine Monophosphate Analogs as Inhibitors of Thymidylate Synthases, and as Substrates or Inhibitors of Thymidine Monophosphate Kinase in Mycobacterium tuberculosis, *Chemistry & Biodiversity* **9**, 536-556 (2012).

27. A. Parchina *et al.*, Discovery of an Acyclic Nucleoside Phosphonate that Inhibits Mycobacterium tuberculosis ThyX Based on the Binding Mode of a 5-Alkynyl Substrate Analogue, *ChemMedChem* **8**, 1373-1383 (2013).

28. P. Kuhn *et al.*, Crystal structure of thy1, a thymidylate synthase complementing protein from Thermotoga maritima at 2.25 A resolution, *Proteins* **49**, 142-145 (2002).

29. D. R. Harkness, E. R. Stadtman, Bacterial Degradation of Riboflavin: VI. Enzymatic conversion of riboflavn to 1-ribityl-2,3-diketo-1,2,3,4-tetrahydro-6,7-dimethylquinoxaline, urea, and carbon dioxide, *J. Biol. Chem.* **240**, 4089-4096 (1965).

30. B. Sherry, R. H. Abeles, Mechanism of action of methanol oxidase, reconstitution of methanol oxidase with 5-deazaflavin, and inactivation of methanol oxidase by cyclopropanol, *Biochemistry* **24**, 2594-2605 (1985).

31. M. E. Taga, N. A. Larsen, A. R. Howard-Jones, C. T. Walsh, G. C. Walker, BluB cannibalizes flavin to form the lower ligand of vitamin B12, *Nature* **446**, 449-453 (2007).

32. D. A. Wadke, D. E. Guttman, Hydrolytic behavior of isoalloxazines related to riboflavin II: Kinetics of degradation of 9-methylisoalloxazine in alkaline media, *J. Pharm. Sci.* **55**, 1363-1368 (1966).

33. P. Renz, R. Wurm, J. Horig, Nonenzymatic transformation of riboflavin into 5,6-dimethylbenzimidazole, *Z Naturforsch C.* **32**, 523-527 (1977).

34. L. A. Maggio-Hall, P. C. Dorrestein, J. C. Escalante-Semerena, T. P. Begley, Formation of the Dimethylbenzimidazole Ligand of Coenzyme B12 under Physiological Conditions by a Facile Oxidative Cascade, *Org. Lett.* **5**, 2211-2213 (2003).

35. R. A. Graham, R. A. Meyer, B. S. Szwergold, T. R. Brown, Observation of myo-inositol 1,2-(cyclic) phosphate in a Morris hepatoma by 31P NMR, *J. Biol. Chem.* **262**, 35-37 (1987).

36. R. K. Boyd *et al.*, Glycerol 1,2-cyclic phosphate in centric diatoms. Observation by 31P NMR in vivo, isolation, and structural determination, *J. Biol. Chem.* **262**, 12406-12408 (1987).

37. F. J. Fraiz *et al.*, Enzymic formation of riboflavin 4',5'-cyclic phosphate from FAD: evidence for a specific low-Km FMN cyclase in rat liver, *Biochem. J.* **330**, 881-888 (1998).

38. H. S. Forrest, A. R. Todd, Nucleotide. Part V. Riboflavin-5' phosphate, *J. Chem. Soc.*, 3295-3299 (1950).